

Supplementary Information

Potential-driven surface active structure rearrangement over

FeP@NC towards efficient electrocatalytic hydrogen evolution

Fumin Tang,¹ Hui Su,¹ Xu Zhao,¹ Hui Zhang,¹ Fengchun Hu,¹ Peng Yao,² Qinghua Liu¹, and Weiren Cheng^{1,*}

¹*National Synchrotron Radiation Laboratory, University of Science and Technology of China, Hefei 230029, Anhui, P. R. China*

²*Department of Electronic Science and Technology, University of Science and Technology of China, Hefei 230027, Anhui, P. R. China*

*E-mail: weiren@ustc.edu.cn

S1. Calibration of potential vs Ag/AgCl to RHE.¹

the relation between Ag/AgCl and RHE potential can be calibrated in the high purity H₂ saturated 0.5 M H₂SO₄ electrolyte with a Pt wire as the working electrode. With a scan rate of 1 mV/s, the average potential, where the current density started to come across X axis (becoming zero) in CV curves, was regarded as the thermodynamic potential for the hydrogen electrode reactions (Figure S2).

S2. Calculation of j_{ECSA} and TOF (Figure S9).^{2,3}

$$ECSA = \frac{C_{dl}}{C_s} \quad (1);$$

$$j_{ECSA} = \frac{j \times S}{ECSA} \quad (2);$$

$$TOF = \frac{j \times S}{2nF} \quad (3).$$

ECSA is short for electrochemical active surface area;

C_{dl} and C_s is double layer capacitance and specific capacitance of samples, and C_s is assumed to 35 $\mu\text{C}/\text{cm}^2$ according to previous report³.

j , S , F and n is the current density under given overpotential, the surface area of the electrode, Faraday constant and the mole number of active metal atoms for the electrode.

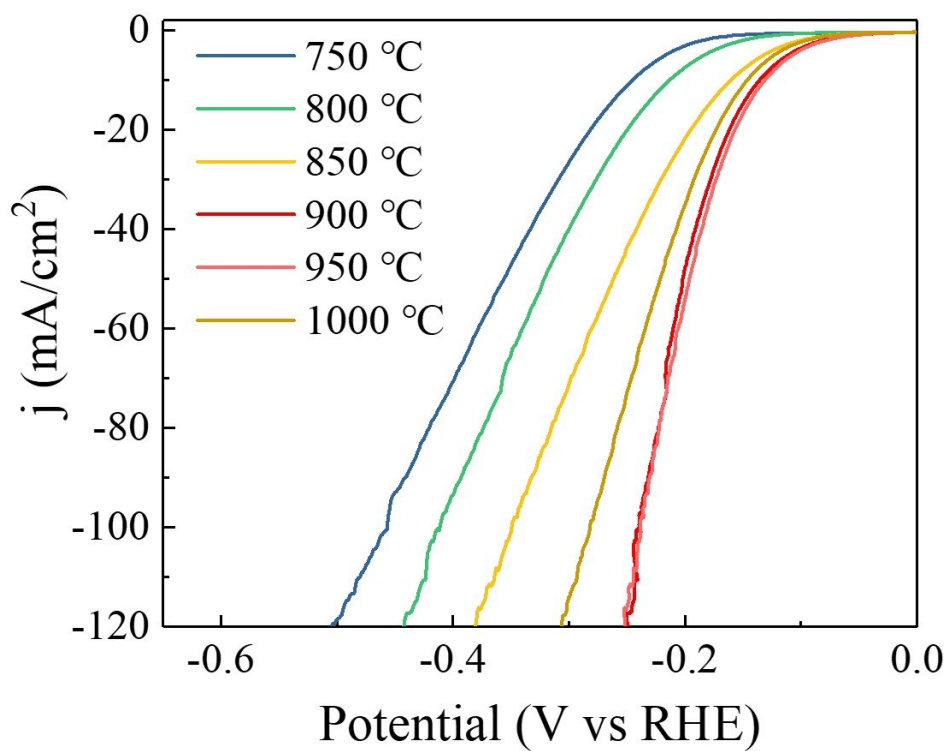


Figure S1. LSV curves in 0.5 M H₂SO₄ for FeP@NC synthesized under different temperatures.

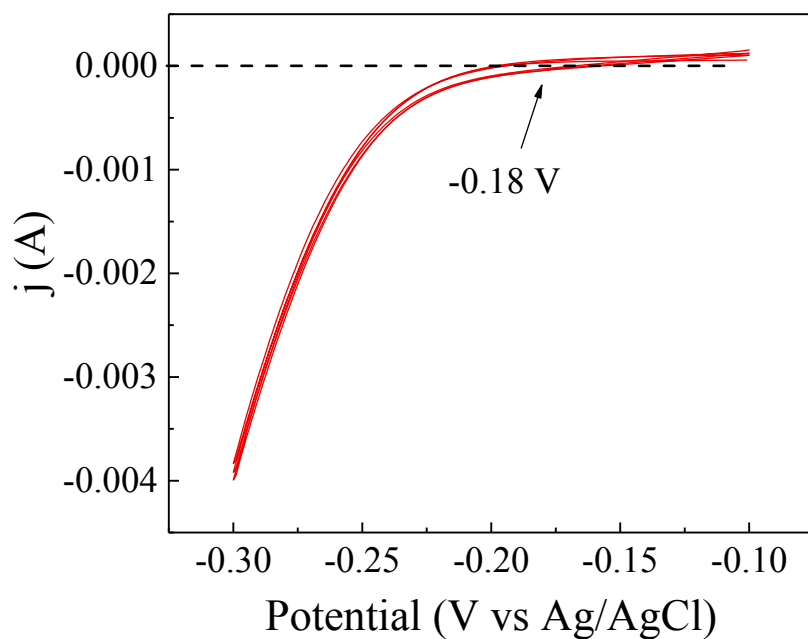


Figure S2. CV curve of Pt wire in 0.5 M H₂SO₄ electrolyte.

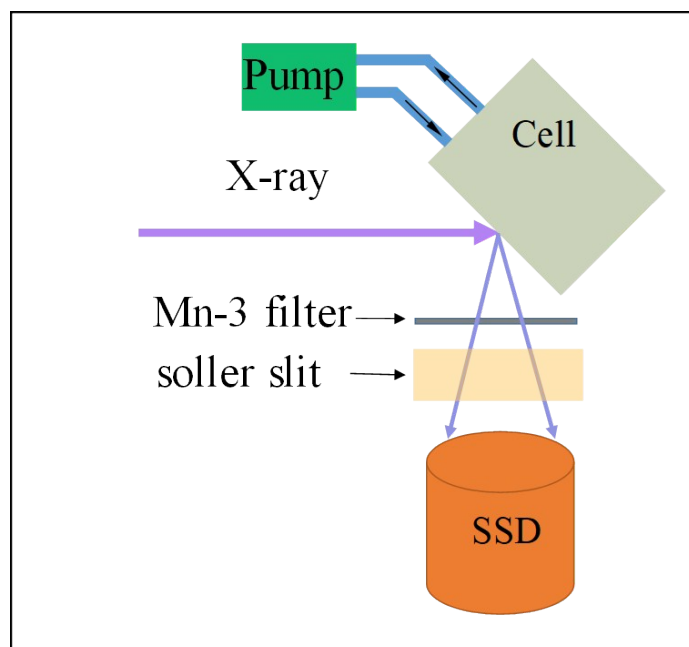


Figure S3. Details of the device in in-situ XAS measurement.

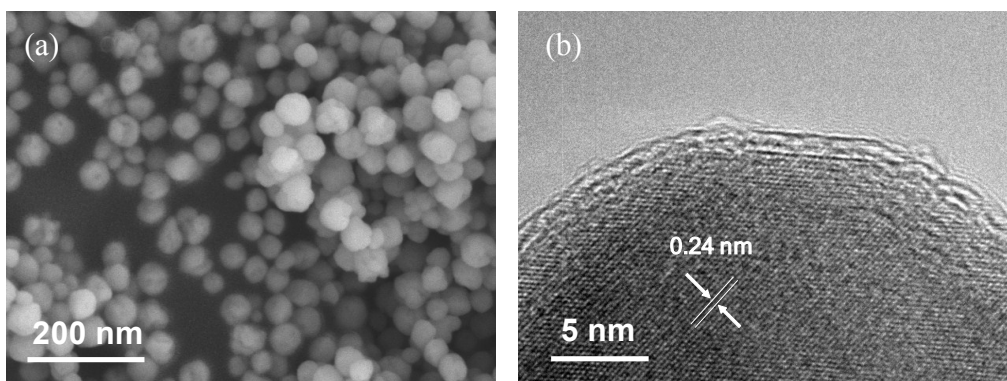


Figure S4. SEM and HRTEM images of FeP particles.

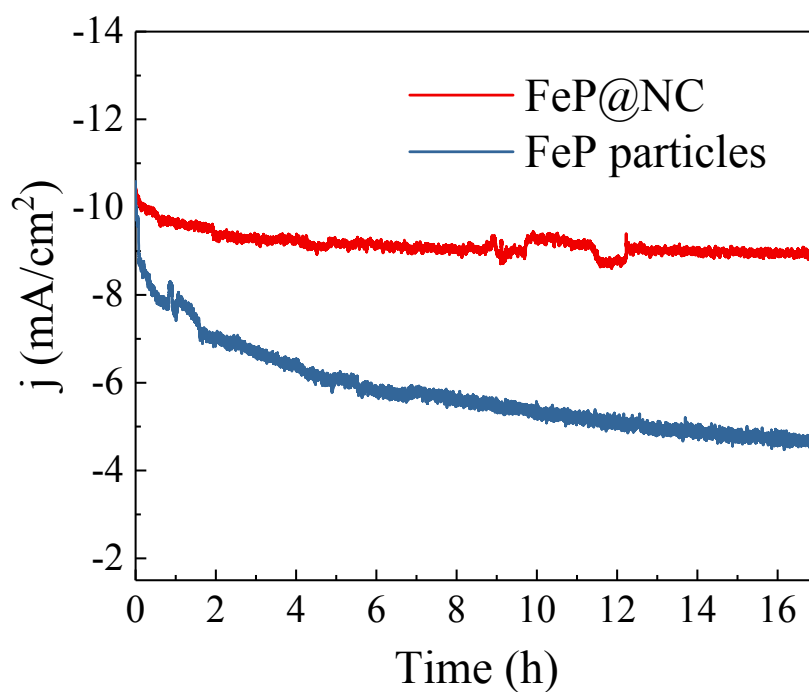


Figure S5. Chronopotentiometric measurements with an initial current density of 10 mA/cm² for FeP@NC at -0.135 V_{RHE} and for FeP particles at -0.495 V_{RHE}.

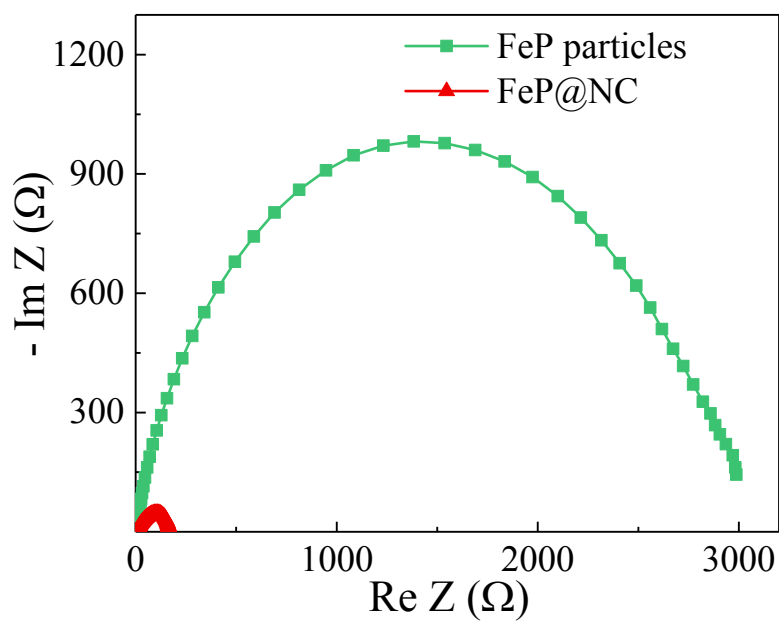


Figure S6. Nyquist plots of FeP particles and FeP@NC at $-0.15 V_{\text{RHE}}$ in a large scale.

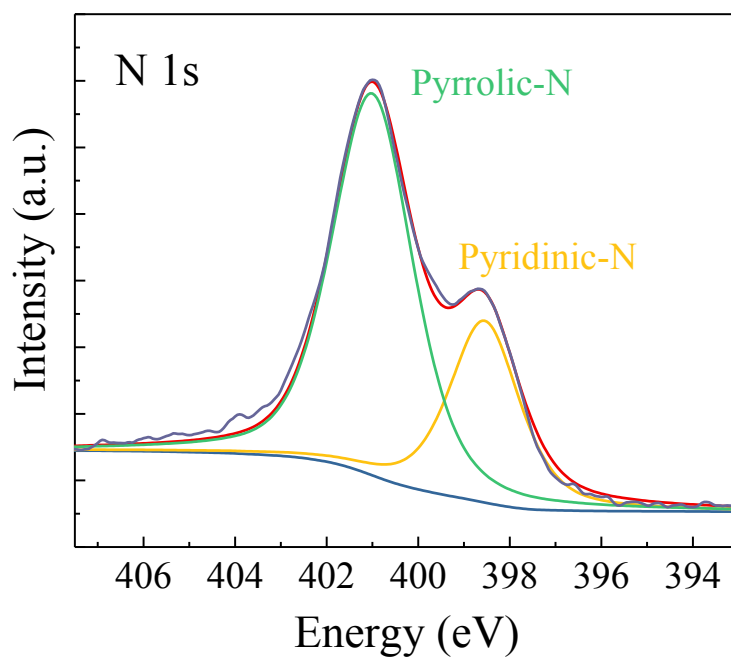


Figure S7. Deconvolution of N 1s XPS spectra for FeP@NC.

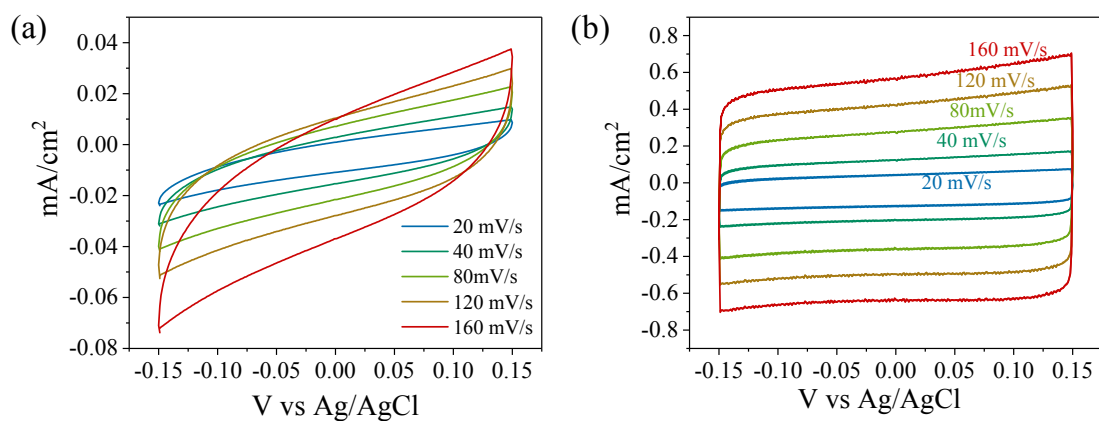


Figure S8. Cyclic voltammetry curves of (a) FeP particles and (b) FeP@NC.

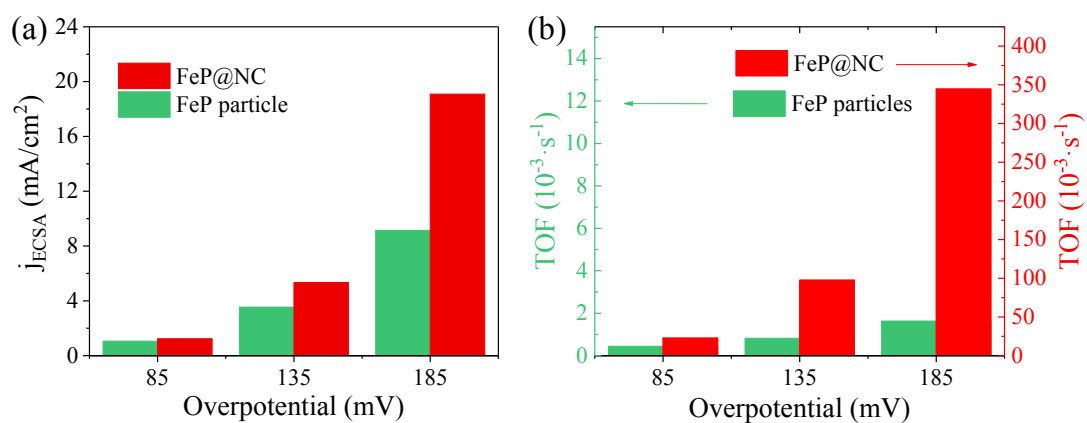


Figure S9. (a) J_{ECSA} , and (b) TOF comparison of FeP@NC and FeP particles under different overpotentials in 0.5 M H_2SO_4 .

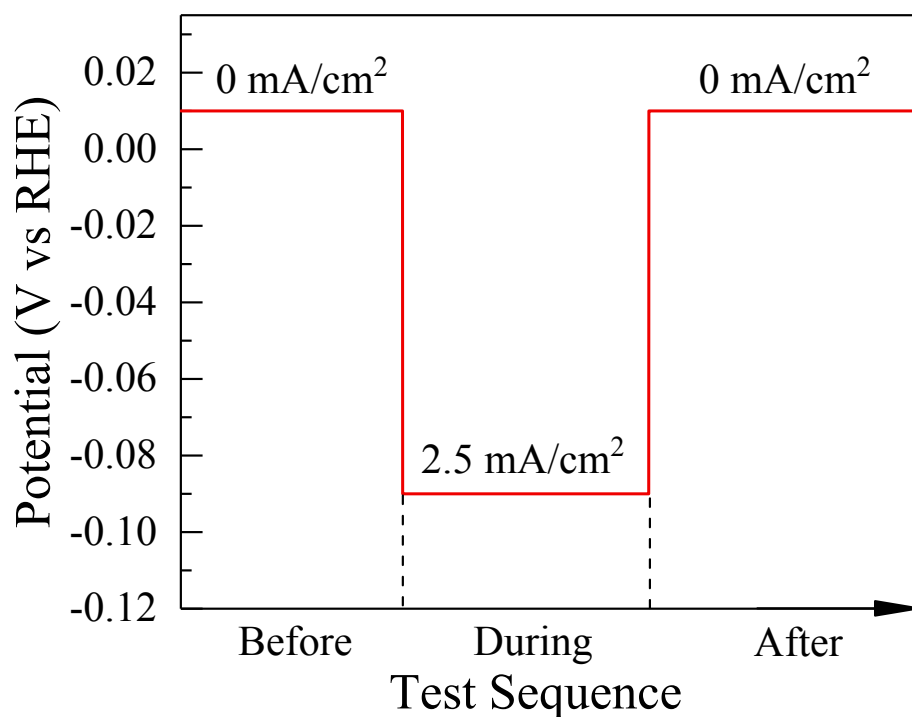


Figure S10. Working condition of work electrode during in-situ XAS measurement.

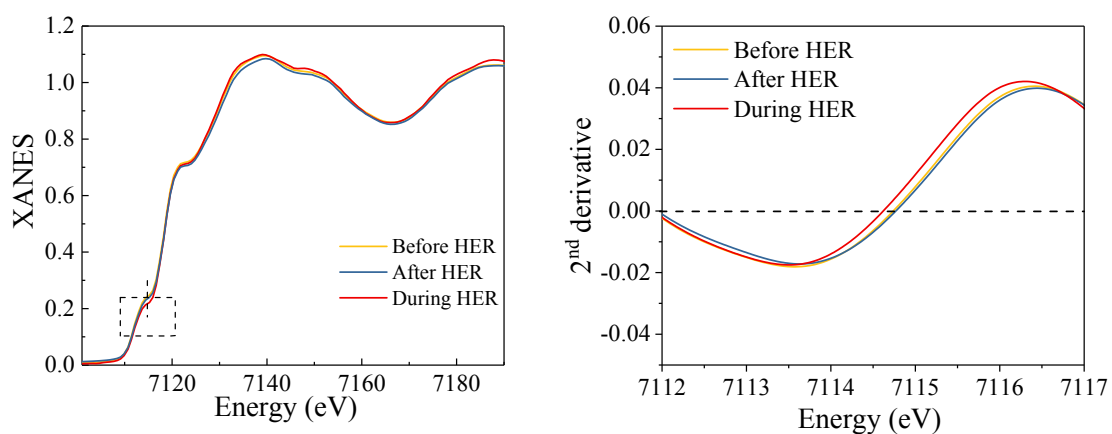


Figure S11. (a) XANES and (b) 2nd derivative curves of pre-edge region.

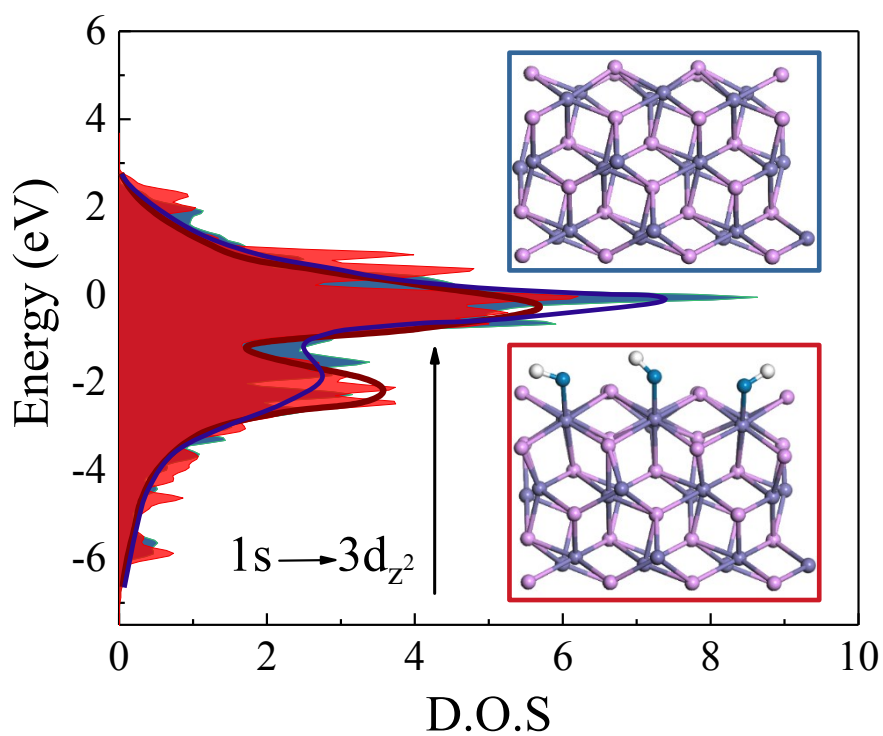


Figure S12. DOS calculation of $3d_{z^2}$ orbitals in different surface structure.

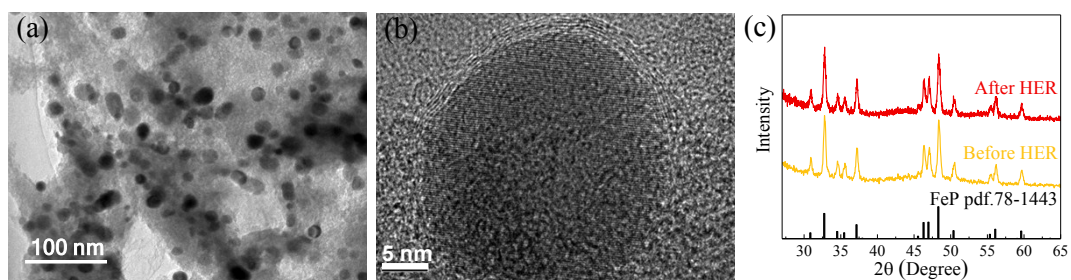


Figure S13. (a) TEM, (b) HRTEM images and XRD patterns of FeP@NC after long-time HER measurement.

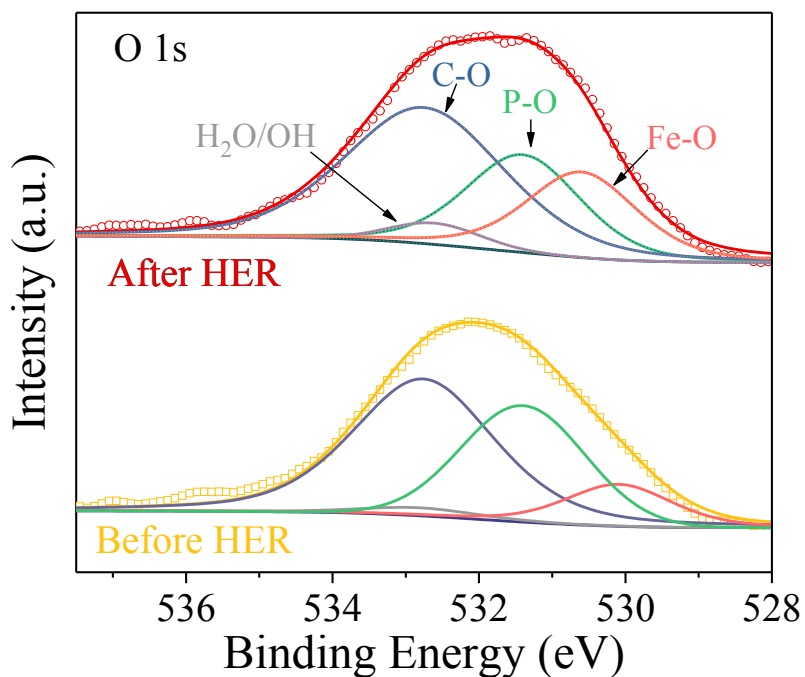


Figure S14. XPS comparison of O 1s for FeP@NC.

Table S1. The EXAFS fitted results for structure parameters around Fe atoms.

| | Paths | N | $\sigma^2 (10^{-3})$ | $\Delta E (eV)$ | $\Delta R (\text{\AA})$ |
|---------------|-------|-------|----------------------|-----------------|-------------------------|
| Before HER | Fe-P | 5.6 | 6.4 | -1.84 | 0.024 |
| | Fe-O | <0.05 | | | |
| During HER | Fe-P | 5.8 | 5.3 | -1.55 | 0.039 |
| | Fe-O | 0.85 | 5.5 | -2.12 | -0.04 |
| After HER | Fe-P | 5.6 | 6.3 | -1.84 | 0.024 |
| | Fe-O | 0.23 | 5.0 | -3.25 | -0.04 |

Table S2. The ratio of different bonds according to Figure S14.

| | Fe-O | P-O | C-O | H ₂ O/OH |
|------------|--------|--------|--------|---------------------|
| Before HER | 12.0 % | 32.9 % | 52.7 % | 2.4 % |
| After HER | 22.1 % | 24.9 % | 49.7 % | 3.3 % |

Table S3. Summary of HER performance for recent typical TMP electrocatalysts in 0.5 M H₂SO₄ electrolyte.

(Stability is defined as the time when current density decays to its' 90 %)

| | $\eta@10$ mA/cm ² (mV) | Tafel slope (mV/dec) | Stability | Ref. |
|--------------------------------------|---|----------------------------|-----------|---|
| FeP@NC | 135 | 78 | >15 h | This work |
| FeP | 240 | 67 | - | Chem. Commun., 2013, 49, 6656. |
| FeP/NCNSs | 114 | 64 | - | ACS Sustain. Chem. Eng., 2018, 6, 11587- 11594. |
| FeP nanowires | 96 | 39 | < 1 h | Chem. Commun., 2016, 52, 2819–2822. |
| CoP nanorod bundle arrays/Ti | 203 | 40 | ~10 h | Electrochem. Commun., 2015, 56, 56–60. |
| CoP@BCN-1 | 87 | 46 | < 10 h | Adv. Energy Mater., 2017, 7, 1601671. |
| Ni-P@Carbon fiber paper | 98 | 58.8 | - | Adv. Funct. Mater., 2016, 26, 4067–4077. |
| Ni ₃ P porous hollow | 85 | 50 | > 11 h | J. Mater. Chem. A, 2016, 4, 10925–10932. |
| Ni ₂ P nanoparticles | 172 | 62 | < 6 h | RSC Adv., 2015, 10290– 10295. |
| MoP ₂ nanoparticles/Mo | 143 | 57 | - | Nanoscale, 2016, 8, 8500–8504 . |
| MoP nanosheet array | 124 | 58 | < 10 h | Appl. Catal. B: Environ., 2016, 196, 193–198 |

References

1. Li Y.Y., *J. Am. Chem. Soc.*, 2011, **133**, 7296-7299.
2. Liu B. et al, *Adv. Mater.*, 2018, **30**, 1803144.
3. McCrory C. C. L., *J. Am. Chem. Soc.*, 2013, **135**, 16977–16987.